Analytica Chimica Acta 1317 (2024) 342906

Contents lists available at ScienceDirect

Analytica Chimica Acta

journal homepage: www.elsevier.com/locate/aca

Unveiling compositional images of specific proteins in individual cells by LA-ICP-MS: Labelling with ruthenium red and metal nanoclusters

Paula Menero-Valdés [a], Lydia Álvarez [b], Héctor González-Iglesias [c], Beatriz Fernández [a,*], Rosario Pereiro [a]

[a] Department of Physical and Analytical Chemistry, University of Oviedo, Faculty of Chemistry, Avda. Julián Clavería 8, 33006, Oviedo, Spain
[b] Fundación de Investigación Oftalmológica (FIO), Avda. Dres. Fernández-Vega, 34, 33012, Oviedo, Spain
[c] Instituto de Productos Lácteos de Asturias, Consejo Superior de Investigaciones Científicas (IPLA-CSIC), Villaviciosa, Spain

HIGHLIGHTS

- Concentration of proteins within individual cells was obtained by LA-ICP-MS.
- The simultaneous analysis of a specific protein and the cell volume was achieved.
- Ruthenium red was employed as a cell volume marker.
- AuNCs were used as specific antibody labels to develop metal immunoprobes.
- CYP1B1 was quantified in ARPE-19 cells under control and oxidative stress conditions.

GRAPHICAL ABSTRACT

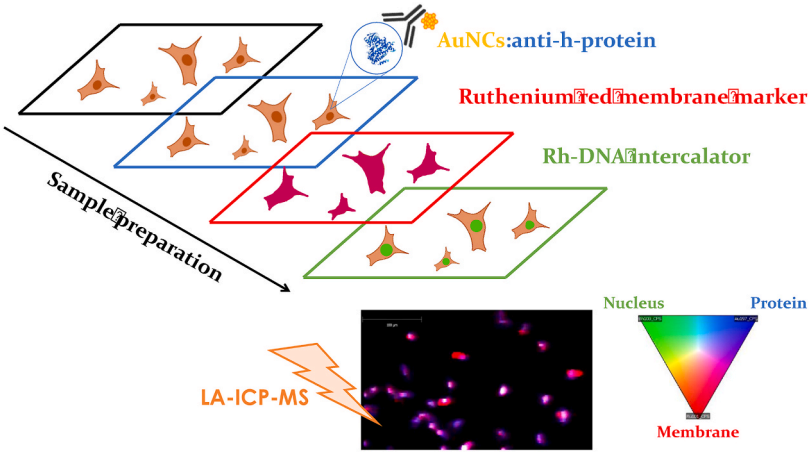

ARTICLE INFO

Handling Editor: Dr. L. Liang

Keywords:
Laser ablation ICP-MS
Metal nanoclusters
Antibody labelling
Cytosolic proteins
Quantitative distribution of proteins

ABSTRACT

Background: Recent biological studies have demonstrated that changes can occur in the cellular genome and proteome due to variations in cell volume. Therefore, it is imperative to take cell volume into account when analyzing a target protein. This consideration becomes especially critical in experimental models involving cells subjected to different treatments. Failure to consider cell volume could obscure the studied biological phenomena or lead to erroneous conclusions. However, quantitative imaging of proteins within cells by LA-ICP-MS is limited by the lack of methods that provide the protein concentration (protein mass over cell volume) rather than just protein mass within individual cells.

Results: The combination of a metal tagged immunoprobe with ruthenium red (RR) labelling enables the simultaneous analysis of a specific protein and the cell volume in each cell analyzed by LA-ICP-(Q)MS. The results indicate that the CYP1B1 concentration exhibits a quasi–normally distribution in control ARPE-19 cells, whereas AAPH–treated cells reveal the presence of two distinct cell groups, responding and non–responding cells

* Corresponding author.
E-mail address: fernandezbeatriz@uniovi.es (B. Fernández).

https://doi.org/10.1016/j.aca.2024.342906
Received 28 February 2024; Received in revised form 29 May 2024; Accepted 23 June 2024
Available online 25 June 2024

to an *in vitro* induced oxidative stress. The labelling of the membrane with RR and the measurement of Ru mass in each cell by LA-ICP-MS offers higher precision compared to manually delimitation of the cell perimeter and eliminates the risk of biased information, which can be prone to inter–observer variability. The proposed procedure is fast and minimizes errors in cell area assignment and offers the possibility to carry out a faster data treatment approach if just relative volumes are compared, which can be advantageous for specific applications. *Significance and novelty:* This work presents an innovative strategy to directly study the distribution and concentration of proteins within individual cells by LA-ICP-MS. This method employs ruthenium red as a cell volume marker and Au nanoclusters (AuNCs) tagged immunoprobes to label the protein of interest. Furthermore, the proposed labelling strategy enables rapid data processing, allowing for the calculation of relative concentrations and thus facilitating the comparison across large datasets. As a proof–of–concept, the concentration of the CYP1B1 protein was quantified in ARPE-19 cells under both control and oxidative stress conditions.

1. Introduction

The analysis of proteins in biological samples has gained great importance in recent years aiming to discover biomarkers, therapeutic targets, and altered pathways of many diseases. In this context, cellular models are interesting samples to study disease pathogenesis and evaluate drug responses [1]. However, it is crucial to consider the evaluation of the cell heterogeneity when analyzing cell populations. Even genetically identical cells show variations in elemental and biomolecular levels [2,3]. Therefore, the analysis of specific proteins in cell cultures in a cell–by–cell basis will provide accurate biological information [4,5]. Additionally, it is essential to consider the volume of each cell to comprehend cellular dynamics. Cell volume can be influenced by various factors, including the cell cycle stage and external stimuli [6]. Recent articles also highlight size–dependent changes in the proteome [7]: some proteins may alter their concentration because of changes in cell size [8]. Therefore, it would be biologically relevant to determine not only the mass of target proteins but also their concentration (taking into account cell volume) in individual cells.

Inductively coupled plasma – mass spectrometry (ICP-MS) is a highly valuable analytical tool for monitoring individual entities, such as cells, when proper sample introduction systems are used [9–11]. The single cell (sc) nebulization approach coupled to ICP-MS enables the study of specific proteins within individual cells if the sought biomolecules are properly labelled with metal–tagged specific antibodies [12]. This combination offers advantages, such as low limits of detection, high multiplexing capabilities, and the possibility of monitoring endogenous elements in each cell. Recent studies employing sc-ICP-MS with a time of flight (ToF) analyzer have focused on determining each cell's volume [13,14]. This approach allows for the calculation of the concentration of specific proteins per cell, not just their mass. Ruthenium red (RR), a polysaccharide–specific stain, has been proposed as a cell surface marker for detecting cells in suspensions, showing its potential as label for the determination of cell volume by sc-ICP-ToFMS [13,15]. However, it is important to note that sc-ICP-ToFMS provides only relative changes in cell volume (and, consequently, relative concentration of target proteins [15]). To obtain precise measurements of absolute cell volume, microscopic measurements are necessary. However, it is not possible to measure the exact same cells using both sc-ICP-MS and microscopy [13]. In addition, instruments like ICP-ToFMS are not commonly available in many laboratories.

The coupling of a laser ablation (LA) system to ICP-MS enables the acquisition of compositional images of biological tissues [16–19] and individual cells [20]. Endogenous elements can be directly measured by LA-ICP-MS, while the analysis of biomolecules requires proper labelling with detectable tags. Metal nanoclusters (MNCs) emerge as highly promising tags for such purposes due to the combination of small size (below 3 nm) and a high signal amplification [21]. Moreover, when employing LA-ICP-MS the cell transport efficiency (TE) is not size–biased, in contrast to nebulization sc-ICP-MS [22]. Several approaches have been proposed for the quantification of different analytes in cells (e.g., endogenous metals, nanoparticles–NPs, and biomolecules) by LA-ICP-MS [23]. Authors have tackled the lack of reference materials for LA-ICP-MS by using in–house calibration standards which try to simulate the cell matrix, such as gelatins [20,24], nitrocellulose membranes [25,26] or rhodamine microdroplets [27]. A fully matrix–matched calibration was achieved by Lores-Padin et al. using the same cell line as matrix and standards [28]. Isotope dilution has been also employed for the determination of gold NPs in cells [29] and Luo et al. evaluated the use of particulate AuNPs standards [30]. However, there is a lack of methods which allow for the determination of cell volume, and thus the determination of analyte concentration within the cells, not just the mass. Van Malderen et al. propose a strategy to reconstruct the 3D distribution of tags in cells but LA-ICP-MS needs to be combined with micro-computer tomography [31].

This work presents an innovative approach for determining the distribution and concentration of specific proteins in individual cells using LA coupled with quadrupole (Q) ICP-MS. A specific antibody (Ab) tagged with NCs composed of several hundred gold atoms (AuNCs) was employed to label the target protein, while the cell membrane was labelled with RR. As a proof–of–concept, the concentration of the CYP1B1 protein was quantified in the human retinal pigment epithelium (RPE) cell line, ARPE-19 [32], under pro–oxidative stress induced by 2, 2′-azobis(2-methylpropionamidine) dihydrochloride (AAPH) treatment, along with control conditions.

CYP1B1, an enzyme member of the CYP1 subfamily of the cytochrome P450 superfamily which can be localized in cellular eye tissues, shows several functions, including the modulation of oxidative stress and activation of NF-κB [33]. Recent studies indicate that the absence of CYP1B1 leads to increased levels of reactive oxygen species (ROS) in mice [34] and *in vitro* human retinal endothelial cells [35]. Thus, in this study, CYP1B1 concentration was determined on a cell–to–cell basis using LA-ICP-(Q)MS, underscoring the importance of considering individual cell volume when working with cell cultures.

2. Materials and methods

In this study, a novel approach is proposed to determine CYP1B1 in individual ARPE-19 cells by LA-ICP-(Q)MS. For such purpose, AuNCs were employed as a specific tag to label the Anti-h-CYP1B1 Ab, and RR was assessed to account for cell volume. In addition to LA-ICP-MS measurements, optimization studies for determining Ab concentration in the immunoprobe were conducted using sc-ICP-MS and fluorescence. The Supplementary Material provides detailed information on the chemicals and materials used, the immunocytochemistry (ICC) protocols for fluorescence microscopy, sc-ICP-MS, and LA-ICP-MS analyses, as well as experimental conditions used for the analysis of ARPE-19 cells in suspension by sc-ICP-MS.

2.1. Experimental methods

2.1.1. ARPE-19 Cell culture and pro-oxidative stress treatment

ARPE-19 cells were cultured in supplemented DMEMF12 medium (1 % P/S and 10 % FBSi) at 37 °C and 5 % CO_2. ARPE-19 cells used for optimization procedures were cultured in Corning cell culture flasks for sc-ICP-MS measurements and in 96-well microplates for ICC and

confocal microscopy experiments. Cells for sc-ICP-MS were mild–fixed with 4 % PFA following a previous optimized protocol [l4]. For LA-ICP-MS analysis, cells were cultured in chambers at a density of $5{\cdot}10^3$ cells/well in DMEMF12 (1 % P/S and 10 % FBSi). After 24 h, the medium was changed to DMEMF12 (1 % P/S and 2 % FBSi). Then, 24 h later, cells were either treated or non-treated with 2 mM AAPH in culture medium for another 24 h. Cells were fixated with a 20 min incubation in 4 % PFA and stored at 4 °C until further use.

Concerning treatment inducing oxidative stress, the concentration of AAPH was optimized using an assay determining ROS production and a viability assay. Cells were cultured in two 96-well microplates ($3{\cdot}10^3$ cells/well) in DMEMF12 (supplemented with 1 % P/S and 10 % FBSi). After 24 h, the medium was changed to DMEMF12 (supplemented with 1 % P/S and 2 % FBSi). After additional 24 h in such medium, various AAPH concentrations ranging from 0 to 5 mM were added to ARPE-19 cells for 24 h. The viability of the treatment was studied in one plate with a CyQuant proliferation assay following the instructions of the manufacturer. The other plate was used to determine the ROS levels; the cells were treated with 10 μM H_2DCFDA and incubated for 30 min. Fluorescence emission was measured with a microplate reader.

2.1.2. Cell labelling for determination of protein concentration

The analysis of a specific protein by LA-ICP-MS requires a preceding labelling procedure with a detectable tag. In this study, CYP1B1 targeted biomolecules within each cell were labelled using immunoprobes tagged with AuNCs (Anti-h-CYP1B1:AuNCs). Furthermore, in a sequential step RR was employed to stain ARPE-19 cell membranes for the assessment of cell volume (i.e., AuNCs and RR labelling procedures were not performed simultaneously).

For specific protein labelling with the AuNCs immunoprobe, the bioconjugation of AuNCs to the CYP1B1 Ab was performed following a previously optimized protocol [36]. A molar ratio of Anti-h-CYP1B1: AuNCs of 1:5 was used in the bioconjugation reaction. The optimal Ab concentration in the immunoprobe employed in ICC protocols for LA-ICP-MS analysis was determined through fluorescence and sc-ICP-MS. Details regarding ICC protocols and the experimental procedure for sc-ICP-MS and fluorescence measurements are also provided in the Supplementary Material.

On the other hand, RR was used for membrane cell labelling to account for individual cell volume. RR labelling conditions were optimized in terms of RR concentration and the most appropriate solvent to ensure reproducible cell labelling. In addition, it is necessary to avoid unspecific interactions of RR with the microscope slide coating as well as to ensure successful removal of the added RR excess. First, chambers without cells were treated for 30 min with 0.4 mL of different RR solutions (1, 5, 10, or 25 μg mL^{-1}), each prepared in different solvent conditions: 0.1 M PBS (pH 7.4), and ultrapure water at pH 5.8, 5.0, and 4.5 adjusted with HCl. Subsequently, the chambers were disassembled and washed by immersing them in the respective solvent for 30 min. The slides were then observed under the LA camera and photographed. Second, to determine the order to be followed for membrane and protein labelling (using RR and Anti-h-CYP1B1:AuNCs immunoprobe, respectively), ARPE-19 cells were fixated on 8-well Nunc Lab Tek Chamber Slides. These chamber slides utilized are dismountable. Following the desired cell treatment, the chamber can be detached, leaving a slide with the attached cells intact. Different wells in a chamber slide with fixed cells were treated with 0.4 mL of 0.5, 1, 5, or 10 μg mL^{-1} RR in acidified ultrapure water at pH 5 for 30 min. The wells were washed twice with ultrapure water (pH 5) using a micropipette, and then the cells were treated following the ICC protocol described in the Supplementary Material. Also, a different chamber slide (containing wells with fixed cells) was subjected first to the ICC protocol and then labelled with 0.4 mL 0.5, 1, 5, or 10 μg mL^{-1} of RR in acidified ultrapure water (pH 5) for 30 min. Then, chamber slides were disassembled, and the slides were washed by immersion in pH 5 ultrapure water for 30 min. Both slides were stored in PBS until analyzed by LA-ICP-MS.

2.1.3. Preparation of LA-ICP-MS in–house standards

Quantification of Ru and Au in ARPE-19 cells by LA-ICP-MS was conducted using gelatins as standards, with the assumption that gelatin density (1.14 g cm^{-3}) is comparable to cell density. To prepare the standards, gelatin (15 % w/w) was mixed with different amounts of RR and $AuCl_4Na{\cdot}H_2O$ aqueous solutions, heated (60 °C) with stirring for 15 min, and then the solutions were immediately frozen at −20 °C in the cryostat to form small gelatin beads, which were stored at −80 °C. For Ru and Au determination in each gelatin standard (standards in the range of 0–200 μg g^{-1} for Ru and Au), gelatins were submitted to an acid digestion and were analyzed by conventional nebulization ICP-MS.

In the proposed analytical procedure, it is crucial for the gelatin thickness to match the ARPE-19 cell thickness, which must be previously determined. Confocal microscopy was employed for such purpose. APOE, a protein uniformly distributed in the cell cytosol [37], was used to label ARPE-19 cells (detailed protocol in Supplementary Material), and fluorescence images of individual cells were obtained using a confocal microscope. Consequently, the ARPE-19 cell average thickness (fixed on the slides) was experimentally determined in the central region of the cell, and the gelatin standards were cut into sections of the same thickness as ARPE-19 cells and mounted on glass slides.

2.2. Instrumentation: LA-ICP-MS and sc-ICP-MS measurements

The ICP-(Q)MS employed for measurements was a 7900 series (Agilent). For LA-ICP-MS analysis, the NWR193 excimer–based system (Elemental Scientific, Inc. – ESI) equipped with a TwoVol2 ablation cell and DCI interface (both from ESI) were used. To achieve high–resolution analysis of individual ARPE-19 cells, we utilized a multiple line scanning mode with a spot size of 2 μm (2 × 2 $μm^2$, squared shape). A laser pulse frequency of 20 Hz and a laser fluence of 0.3 J cm^{-2} ensured the quantitative ablation of the entire cell volume (Table S1 outlines the optimized experimental conditions for both ICP-(Q)MS and LA instruments and Fig. S1 depicts qualitative images with the optimized parameters). Slides with ARPE-19 cells were washed with ultrapure water before being analyzed. In the case of the gelatin standards, they were measured by LA-ICP-MS before every cell imaging. The data processing, including the generation of images depicting the distribution of $^{101}Ru^+$ and $^{197}Au^+$ in individual ARPE-19 cells, calibration curves, background subtraction, and the selection of cell regions (i.e., delimitation of cell perimeter of each cell), was performed using iolite (v4) software (ESI). Thermal gradient was chosen as the scale for images, and an expand by interpolating filter was applied for data treatment.

A microFAST Single Cell Introduction System (ESI) was employed for sc-ICP-MS analysis of cell suspensions. The sc introduction system includes an autosampler, a CytoNeb nebulizer, a CytoSpray chamber, and a one-piece torch. Table S2 collects the experimental conditions used for the analysis of ARPE-19 cell suspensions by sc-ICP-MS. A microplate reader (Victor X5, PerkinElmer) was employed for cellular viability and ROS assays. An optical microscope (DM6000B, Leica) equipped with epifluorescence (RGB filter) and a DFC 310 camera, and a confocal microscope (TCS-SP8X, Leica) were used for ICC. Cell counting was done with a Neubauer hemocytometer (Sigma-Aldrich). Statistical tests and data presentation (i.e., charts, histograms, cell event profiles) were carried out with Excel (Microsoft). SPCal software was employed for sc-ICP-MS data. Fluorescence and confocal microscopy images were treated with Image J.

3. Results and discussion

3.1. Optimization of the Cell culture conditions

To determine the optimal AAPH concentration that would increase ROS production in ARPE-19 cells without compromising cell viability, ROS levels and cell viability assays were conducted at different AAPH concentrations (0.5, 1, 2, 3, 4, and 5 mM) during 24 h. As it can be seen

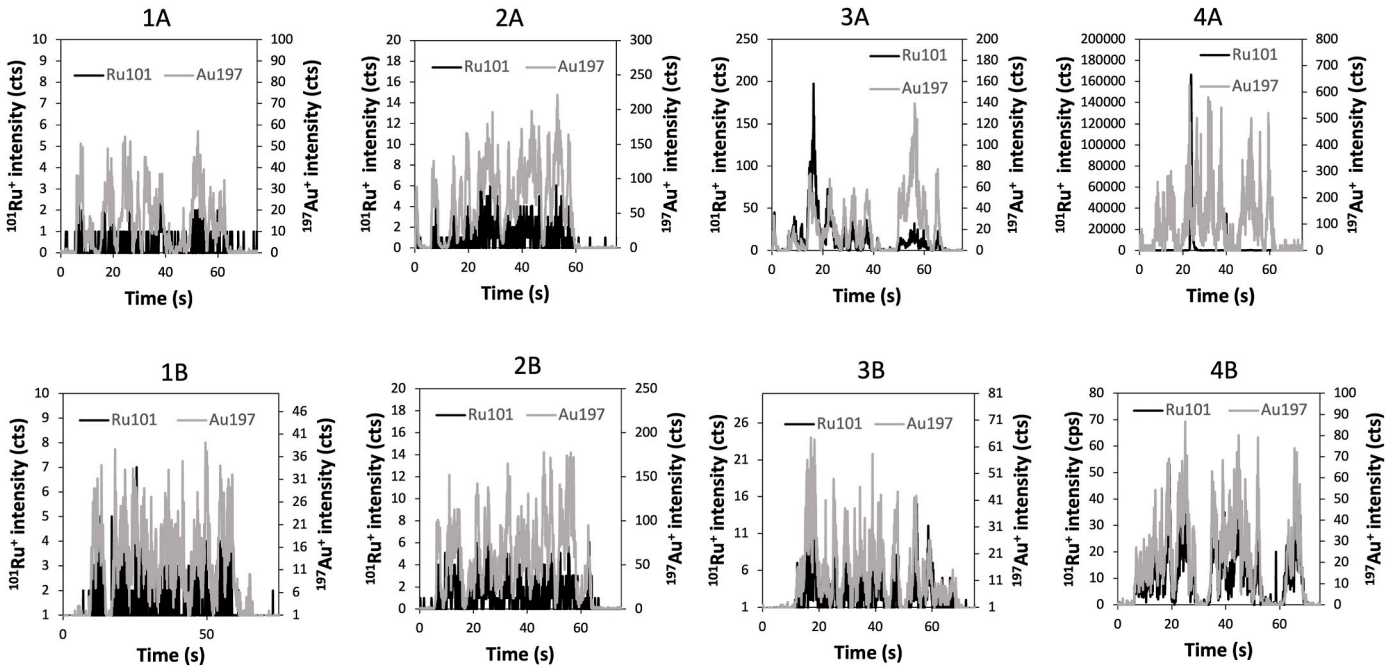

Fig. 1. Line scans measured by LA-ICP-MS of control ARPE-19 cells after labelling. Cells in Slide A were first treated with RR and then with the Anti-h-CYP1B1:AuNCs immunoprobe (denoted with A), while cells in Slide B were first treated with the immunoprobe and then with RR (denoted with B). Different RR concentrations were tested: 0.5 μg mL^{-1} (1), 1 μg mL^{-1} (2), 5 μg mL^{-1} (3), and 10 μg mL^{-1} (4).

in Fig. S2A, the viability of ARPE-19 cells remains above 70 % for all AAPH concentrations assayed; however, variability increases for AAPH concentrations exceeding 2 mM. Regarding ROS production (Fig. S2B), significant differences (*t*-test, p-value <0.01) were observed for all AAPH concentrations compared to control (CT) cells. Considering both experiments, a 2 mM AAPH concentration was chosen for inducing oxidative stress without compromising cell viability and maintaining reproducibility.

3.2. Optimization of the Cell labelling for LA-ICP-MS analysis

In the proposed methodology, the labelling procedure involves two sequential steps: protein labelling using the Anti-h-CYP1B1:AuNCs immunoprobe (for the detection of the target protein via $^{197}Au^{+}$ intensity signal) and cell membrane staining with RR to determine cell volume based on the $^{101}Ru^{+}$ intensity signal.

3.2.1. CYP1B1 labelling with the AuNCs tagged immunoprobe

The optimization of the concentration of the tagged immunoprobe added to ARPE-19 cells is crucial to ensure sufficient Ab for detecting all CYP1B1 proteins in the sample, while also removing excess of the immunoprobe during washing steps. Initially, cells were submitted to an ICC procedure with fluorescence detection (see Supplementary Material). Fluorescence images for each tested Ab concentration are depicted in Fig. S3. Although this detection mode is not quantitative, it can be employed to select the Ab concentration range for further testing by sc-ICP-MS. As illustrated in Figs. S3A and 1 μg mL^{-1} of Ab is insufficient to label CYP1B1 cell protein. On the opposite, an excess of Ab is observed at a concentration of 10 μg mL^{-1} (Fig. S3D), evident from saturated image. Thus, these extreme concentrations were discarded, and the Ab concentration range of 2–5 μg mL^{-1} was chosen for sc-ICP-MS analysis of ARPE-19 cells in suspension.

In a subsequent experiment, fixated ARPE-19 cells in suspension were labelled with the Anti-h-CYP1B1:AuNCs immunoprobe and analyzed by sc-ICP-MS. Details regarding the sample preparation procedure and experimental measurements can be found in the Supplementary Material. Fig. S4 illustrates the average protein concentration per cell at four Ab concentrations. The measured concentration of CYP1B1 in ARPE-19 cells exhibited a significant increase from 2 to 2.5 μg mL^{-1} of Ab and from 2.5 to 3.4 μg mL^{-1} of Ab (*t*-test, *p*-value <0.05 in both cases). However, no significant differences were observed when comparing 3.4 and 5 μg mL^{-1}. Experimental results suggest that below 3.4 μg mL^{-1} there is insufficient Ab to label all the CYP1B1 present in the cells. Therefore, the optimal Ab concentration, ensuring total protein recognition without the risk of residual immunoprobe, was chosen to be 3.4 μg mL^{-1} of Ab.

3.2.2. Cell labelling with ruthenium red

Initially, various experiments were conducted to determine the optimal RR concentration for labeling ARPE-19 cells. Chambers without cells (to account for procedural blanks) were treated with different concentrations of RR (1–25 μg mL^{-1}), using different solvents for RR solution preparation (including PBS, and ultrapure water at pH 5.8, 5, and 4.5). Fig. S5 collects images obtained for each tested condition. As it can be observed, when PBS or ultrapure water at pH 5.8 is used as solvent, RR is not completely dissolved, and undissolved salt spots are evident in the images. An increase in RR concentration (as seen in images denoted with A and B) results in more visible RR spots. Conversely, lowering the pH enhances the solubility of RR, and no spots are observed in the images when dissolving it at pH 5 or 4.5, regardless of RR concentrations. Therefore, pH 5 was selected for cell labelling with RR.

To ascertain the optimal RR concentration for cell labeling and investigate the preferred labeling sequence – whether cells should be submitted first to the ICC protocol using the AuNCs immunoprobe and then followed by RR labelling, or *vice versa* – two chamber slides containing fixed cells were labelled for LA-ICP-MS measurements. In chamber slide A, cells were initially treated with the immunoprobe (ICC protocol for CYP1B1 detection), followed by RR at varying concentrations. Meanwhile, in chamber slide B, cells were first exposed to different RR concentrations and then subjected to the ICC protocol. Photographs of these chambers are compiled in Fig. S6. It is noteworthy that when RR labelling was carried out first, visible RR spots are evident at the highest concentration tested Figs. S6–4A.

Individual line scans were conducted in the cell cultures by LA-ICP-

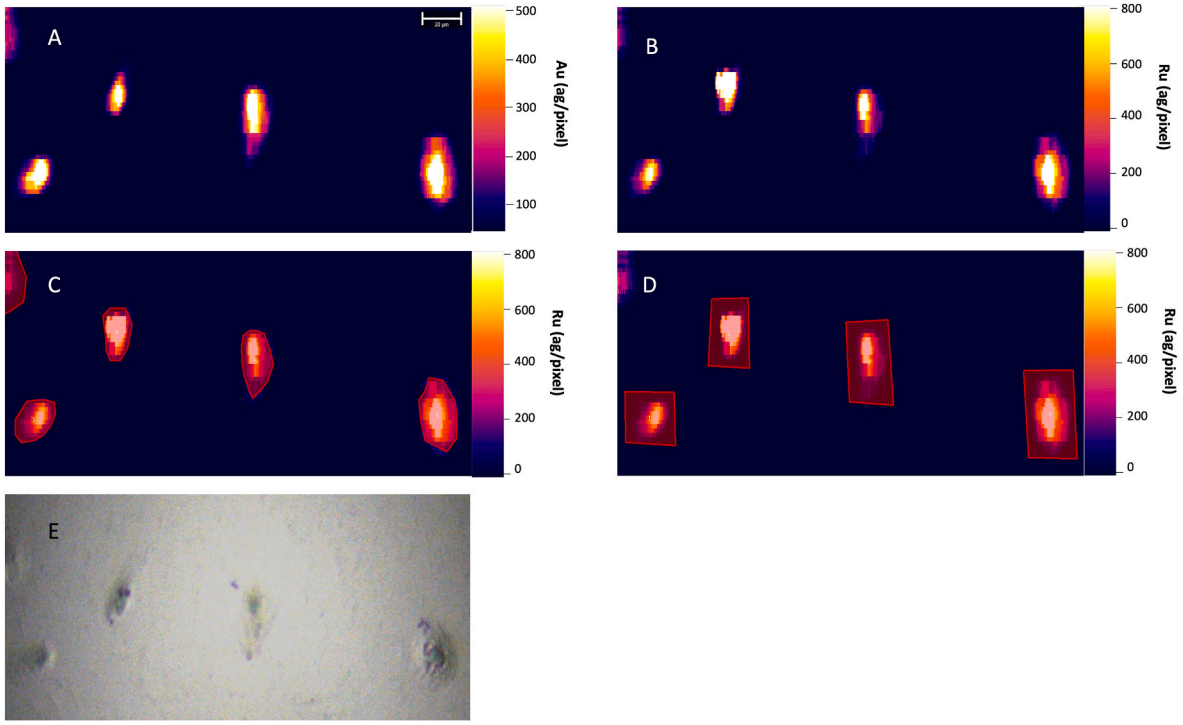

Fig. 2. Quantitative images of control ARPE-19 cells obtained by LA-ICP-MS after labelling CYP1B1 with Anti-h-CYP1B1:AuNCs immunoprobe and the cell membrane with RR. Au distribution (A), and Ru distribution (B). Delimitation of individual cell areas (ROIs) was carried out with Ru mass using two different strategies: drawing polygons ROIs (C), and drawing quadrilateral ROIs (D). Optical image of the ablated region taken with the LA system camera (E).

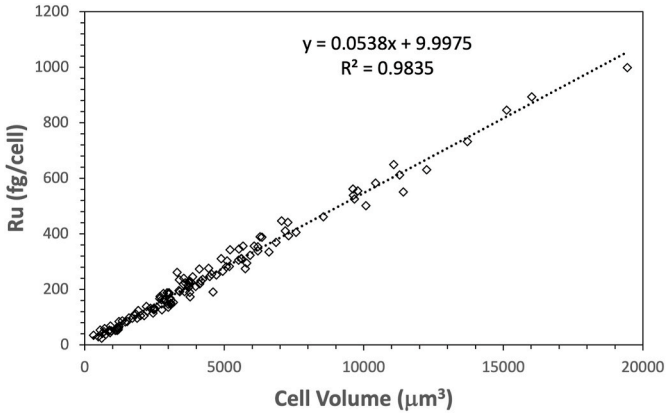

Fig. 3. Scatter plot constructed for ARPE-19 cells analyzed by LA-ICP-MS representing the Ru mass per cell against the cell volume, calculated by integrating Ru mass in quadrilateral ROIs. Both control cells (N = 60), and AAPH treated cells (N = 60) are included.

MS to obtain $^{101}Ru^{+}$ intensity signals from ARPE-19 cells. The results are presented in Fig. 1. In the cell cultures from both slides, the $^{101}Ru^{+}$ intensity increases with the RR concentration used for labelling (within the range of 1–10 μg mL^{-1}). However, unspecific, and highly intense peaks were identified for the highest RR concentration tested in cell cultures from slide A (Figs. 1-4A), probably coming from undissolved RR. This observation aligns with the photographs obtained with the LA camera, where undissolved RR spots are visible in slide A at 10 μg mL^{-1} (Figs. S6–4A). Comparing the $^{101}Ru^{+}$ intensities from the cell cultures of the two slides, the signals are higher for slide A than for slide B when using the same RR concentration. However, there is also a higher background in slide A compared to slide B (e.g., the background at 10 μg mL^{-1} of RR was 5 ± 6 cts and 0.5 ± 0.9 cts for slide A and slide B, respectively). This could be attributed to the washing step after RR labelling. In chamber slide A, the chamber cannot be removed after the RR labelling as the ICC is conducted consecutively, and washing is performed in each well with a micropipette. Conversely, in chamber slide B, RR labelling is the final step, the chamber slides are disassembled, and the slide is washed by immersion. Washing by immersion is likely more thorough and reproducible. Consequently, in subsequent experiments, ARPE-19 cells were first subjected to the ICC protocol with the Anti-h-CYP1B1:AuNCs immunoprobe, followed by labelling with 10 μg mL^{-1} of RR dissolved in ultrapure water (pH 5) and washed by immersion.

3.3. *Calibration using gelatin standards for the individual analysis of ARPE-19 cells by LA-ICP-MS*

In–house gelatin standards, spiked with Au and Ru, were employed for calibration purposes. First, the thickness of ARPE-19 cells fixed on the slides was measured. The goal was to match the thickness of the gelatins and the averaged cell samples, ensuring an equal volume ablation per laser shot for both standards and samples. The thickness of ARPE-19 cells attached to the slide chambers was determined experimentally through confocal microscopy measurements. This involved labelling the cell cytoplasm with Anti-h-APOE and a fluorescence tag (refer to the Supplementary Material for a detailed procedure, and Fig. S7 and Table S3 for experimental results related to confocal microscopy measurements). The average thickness of ARPE-19 cells fixed to the slide chambers was found to be 6.2 ± 0.8 μm (N = 100). The membrane thickness (usually 7.5–10 nm) was disregarded, given its insignificance compared to the uncertainty associated with the gelatin standard thickness when sectioning it with a cryotome. Consequently, gelatin standards were sectioned 6 ± 1 μm slices.

After LA-ICP-MS analysis of gelatin standards, the concentration of Au and Ru (in μg g^{-1}) can be converted into g/pixel. This conversion relied on knowledge of the density of the gelatins (d), the area of the pixel (A), and the gelatin thickness (t), as expressed in **Eq (1)**:

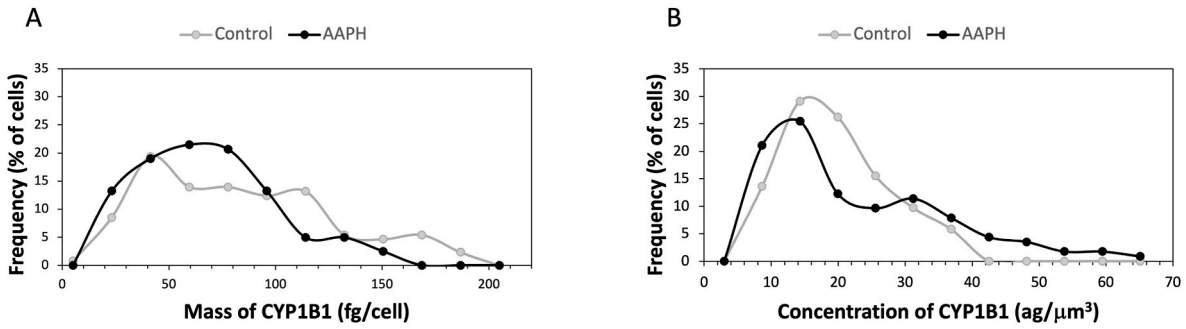

Fig. 4. Mass frequency histogram (in percentage) for CYP1B1 in control (grey line) and AAPH treated (black line) ARPE-19 cells obtained by LA-ICP-MS using Anti-h-CYP1B1:AuNCs immunoprobe and RR labelling. N = 240 (N = 120 for control cells and N = 120 for AAPH treated cells).

$$[Gelatin]\left(\frac{g}{pixel}\right) = [Gelatin]\left(\frac{\mu g}{g}\right) \bullet A\left(\frac{\mu m^2}{pixel}\right) \bullet t\,(\mu m) \bullet d\left(\frac{g}{\mu m^3}\right) \quad \text{Eq. 1}$$

Calibration curves were then constructed representing the intensity per pixel against the mass per pixel for $^{197}Au^+$ and $^{101}Ru^+$ intensity signals. The concentration of the in–house gelatin standards was determined by conventional nebulization ICP-MS (Table S4) and Fig. S8 provides an example of the calibration curves.

3.4. Cell volume calibration with ruthenium red

ARPE-19 cells, subjected to the ICC protocol for CYP1B1 determination (Antih-CYP1B1:AuNCs immunoprobe) and subsequently labelled with RR, were analyzed by LA-ICP-MS under optimized imaging conditions (Table S1). The conditions of the LA system and ICP-MS instrument have been optimized in terms of sensitivity and lateral resolution for the analysis of proteins in individual ARPE-19 cells following both Au intensity signal from AuNCs immunoprobe and Ru from RR labelling. As it can be seen in Fig. S1, images with the optimized parameters maintained the dimensions of the ablated area. Fig. 2 shows the $^{197}Au^+$ and $^{101}Ru^+$ distributions obtained for selected CT ARPE-19 cells (Fig. 2A and B, respectively). The area of each cell was determined with iolite software following $^{101}Ru^+$ intensity signal: an irregular polygon delimiting the cell was manually drawn (Fig. 2C) and the software then yielded the area (in μm^2) within that region of interest (ROI). It is important to note that delineating the cell area without RR labelling (i.e., using the optical image of each cell) introduces a notable source of error due to the poor resolution of the images (see in Fig. S9 and Fig. 2E).

Taking into account experimental measurements carried out by confocal microscopy, ARPE-19 cells have a homogeneous thickness (Table S3: 6.2 ± 0.8 μm, n = 100). Therefore, their shape can be approximated to the shape of an irregular prism, being the prism base the polygon ROI delimited with iolite software and the prism height the cell thickness. Thus, the volume of each cell (V_{cell}) can be determined with the mathematical expression for the volume of an irregular prism (**Eq (2)**):

$$V_{cell} = V_{irregular\ prism} = \text{Area base} \times \text{height} = \text{Area ROI} \times t \quad \text{Eq. 2}$$

where Area ROI is the cell area determined with iolite, and t is the thickness determined by confocal microscopy.

Estimation of the averaged cell volume with this procedure could be done for each ablated cell. However, manual delineation using the $^{101}Ru^+$ intensity signal introduces random errors and is time–consuming. To address these limitations, a more accurate approach for calculating cell volume based on the mass of Ru within each cell is proposed here. The Ru mass per cell was determined by integrating the polygonal ROIs (Fig. 2C) and, subsequently, the mass of Ru per cell was plotted against the cell volume (estimated using Eq. (2)). Fig. S10 depicts the scatter plots obtained for both CT cells (Fig. S10A) and AAPH–treated cells (Fig. S10B). In both cases, a positive linear relationship was found between the Ru mass and the volume of ARPE-19 cells ($r^2 > 0.97$, N = 60). The slopes of both graphs were statistically comparable (*t*-test at 95 % confidence, unequal variances), indicating that Ru mass per cell correlates with cell volume independently of AAPH treatment. Considering the experimental results, a unified calibration curve was constructed with combined data from CT and AAPH–treated ARPE-19 cells (N = 120, Fig. S10C). The linearity of the plot was verified with a correlation *t*-test, yielding a *p*-value of $1{\cdot}10^{-112}$, affirming the data fits to the proposed linear model.

This approach was further explored by roughly delimiting a quadrilateral ROI around each cell (Fig. 2D) and integrating the Ru mass within that area. Interestingly, the Ru mass contained in the quadrilateral demonstrated a proportionality to cell volume (Fig. 3), exhibiting an even higher correlation coefficient compared to polygonal ROIs (Fig. S10C). The improved correlation may be attributed to reduced human errors when defining quadrilateral ROIs. Additionally, employing quadrilateral regions for cell delineation reduces the time required for data analysis, a crucial factor when dealing with large number of cells (especially for assessing biological heterogeneity in cellular models).

The accuracy of both strategies for determining the cell volume (either manually with **Eq (2)** using the $^{101}Ru^+$ intensity signal for each cell or using the equation from the calibration curve in Fig. 3; mass of Ru per cell *vs* cell volume) was evaluated. Four cells were analyzed using both methodologies by the same person on three different days, and the results are summarized in Table S5. The error associated with volume determination using the Ru calibration was more than five times smaller compared to the use of $^{101}Ru^+$ intensity signals. Thus, a volume calibration curve can be established with a representative number of cells, enabling the direct determination of the volume of the remaining cells in the dataset from the Ru mass contained in their quadrilateral ROIs. Moreover, combining RR labelling with LA-ICP-MS allows for the determination of the volume of each individual cell, providing quantitative volumes instead of relative volumes obtained when combining RR with nebulization sc-ICP-MS [15].

The volume calibration curve with RR labelling would probably be applicable to other cell lines as this reagent has been widely employed as a cell membrane marker for electron microscopy since the 1970's, having been employed in different kinds of cells (e.g., yeast, bacteria, plant, and mammalian cells) [38–40]. Regarding its use as a volume marker, it has been previously employed in yeast and algae cells by Quin et al. [13] and in mammalian cells in a previous work by our group [15]. It should be also stated that a RR calibration curve must be constructed for each tested cell line if quantitative volumes are required, as the mass of Ru per cell membrane area is cell line dependent [13]. Nevertheless, a fast data processing approach can be used with the combination of RR labelling and LA-ICP-MS: cells can be delimited with quadrilateral ROIs, and Ru mass per cell is integrated in each ROI. As the mass of Ru is proportional to the cell volume, relative cell volumes can be obtained

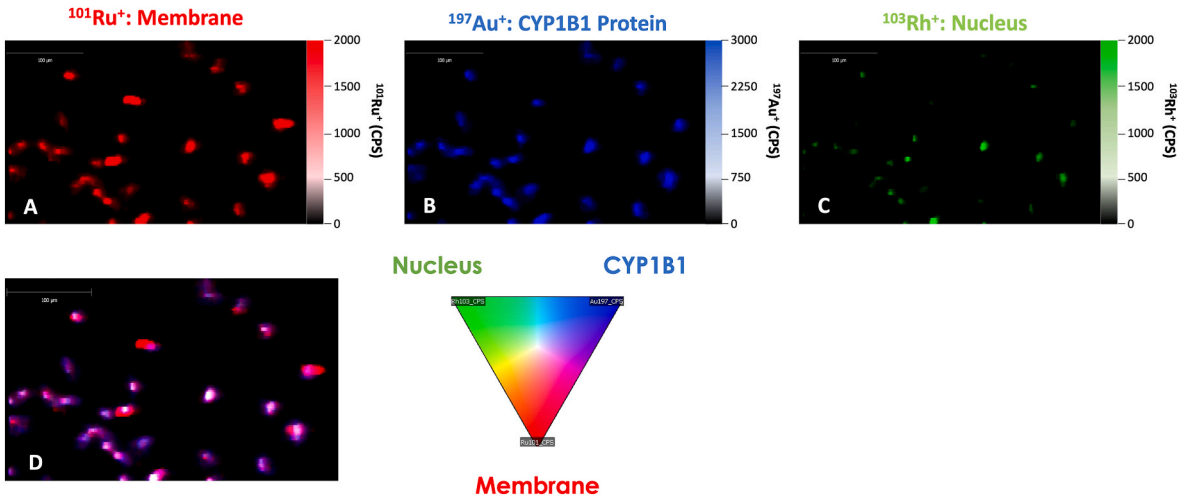

Fig. 5. Qualitative imaging obtained by LA-ICP-MS for control ARPE-19 cells treated with three different labels: RR, Anti-h-CYP1B1:AuNCs, and Rh intercalator. $^{101}Ru^{+}$ distribution shows the localization of the cell membrane (A); $^{197}Au^{+}$ distribution indicates the localization of the protein within the cells (B), $^{103}Rh^{+}$ highlights the cell nuclei (C), and a composite of the three channels ($^{101}Ru^{+}$, $^{103}Rh^{+}$, and $^{197}Au^{+}$) (D).

comparing the mass of Ru contained in each cell. This approach may be sufficient for applications where the same cell line under different conditions is compared.

The obtained results for ARPE-19 cell volumes with the RR volume calibration curve were validated with a different methodology. Control ARPE-19 cells in a dilute suspension were photographed with the camera of an optical microscope capturing random cells in the sample (N = 500). Fig. S11 shows an example of the images taken. The diameter (d) of the cells was determined with Image J software in the photographs. As ARPE-19 cells are spherical in solution, the volume of the cells was calculated with the mathematical formula for determining the volume of a sphere. The comparison between the cell volumes calculated from ARPE-19 diameters in solution and those obtained with the proposed RR calibration is depicted in Fig. S12. The volumes calculated with both approaches were found to be statistically comparable (*t*-test for unequal variances, p-value = 0.26).

3.5. Quantification of CYP1B1 in control and AAPH–treated cells by LA-ICP-MS

CT and AAPH–treated ARPE-19 cells labelled with the Anti-h-CYP1B1:AuNCs immunoprobe and RR were measured by LA-ICP-MS (N = 120 for each condition). The $^{101}Ru^{+}$ and $^{197}Au^{+}$ intensities were converted to metal concentration using the corresponding calibration curves and, thus, the quantitative distribution of Ru and Au within individual cells can be obtained. Next, the Au distribution (in ag/pixel) was transformed into a quantitative CYP1B1 distribution, considering the amplification of the AuNCs immunoprobe [36]. As an example, Fig. S13 illustrates quantitative images for CYP1B1 in ARPE-19 cells for both CT and AAPH groups.

Following the proposed methodology, each cell was delimited with iolite software drawing a quadrilateral region containing the cell (as shown in Fig. 2D). Integrating of all pixels within the delimited region to determine the mass of Ru along with the mass of CYP1B1 in each cell. The volume of each cell was appraised using the RR volume calibration (Fig. 3), and finally the concentration of CYP1B1 per cell was calculated by dividing the mass of the protein by the volume of each cell. In such a way, CYP1B1 was quantified cell by cell in both CT and AAPH-treated cells, and all collected data was represented in frequency histograms to facilitate a comparison of the two experimental conditions. Two frequency histograms were constructed for all ARPE-19 cells: (i) One depicting the percentage of cells within the population that contain a specific mass of CYP1B1 (Fig. 4A), and (ii) Another representing the concentration of CYP1B1 (i.e., dividing the mass of the protein by the volume of each cell; Fig. 4B). Both histograms were constructed with 10 bins, dividing either the mass x–axis (5–188 fg) or the concentration x–axis (3–60 ag μm^{-3}) in 10 data groups. The bin width was proportional to the width of the x–axis (18.2 for the mass histogram and 5.6 for the concentration histogram), allowing for a meaningful comparison despite differences in magnitude on the x-axis.

Regarding the mass of protein per cell (Fig. 4A), a wider distribution was observed for CT cells compared to AAPH–treated cells. However, when looking at the protein concentration (considering cell volume) (Fig. 4B), CT cells displayed a narrower distribution with an almost normal shape, whereas AAPH–treated cells exhibited a broader distribution extending to higher concentrations. The broadness of the mass distribution in the CT cells seems to be corrected when taking into account the cell volume: cells with larger amounts of CYP1B1 were also larger in size. When representing protein concentration, CT cells appeared in a single peak. Nevertheless, the AAPH treatment did not affect all the cells equally. Two cell groups were observed in the concentration distribution, a group of cells showing CYP1B1 concentration similar or lower to CT cells and a group of cells displaying higher concentration of CYP1B1 because of the oxidative stress induced by APPH. Therefore, the different trends found when comparing protein mass or protein concentration illustrate the importance of monitoring not only proteins but also cell volumes when studying the effects of a specific stimulus in a cell population.

3.6. Localization of cellular organelles with RR labelling

Finally, as a proof–of–concept, a sample of CT ARPE-19 cells was sequentially labelled with the Anti-h-CYP1B1:AuNCs immunoprobe (for detecting the CYP1B1 protein), a Rh intercalator to stain the cell nuclei, and RR (to label the cell membrane). Subsequently, ARPE-19 cells were subjected to analysis by LA-ICP-(Q)MS, monitoring $^{101}Ru^{+}$, $^{197}Au^{+}$, $^{103}Rh^{+}$ intensity signals. As it can be observed in Fig. 5, the combined information from these three isotopes allows for the study of the spatial distribution of different components relative to each other.

4. Conclusions

The combination of a metal tagged immunoprobe with RR labelling enables the simultaneous analysis of a specific protein and the cell volume in each cell analyzed by LA-ICP-(Q)MS. Thus, quantitative images of specific proteins in individual cells can be achieved. The results

indicate that the CYP1B1 concentration exhibits a quasi–normally distribution in CT ARPE-19 cells, whereas AAPH–treated cells reveal the presence of two distinct cell groups, responding and non–responding cells to an *in vitro* induced oxidative stress. This reinforces the importance of analyzing cell cultures on a cell–by–cell basis.

The labelling of the membrane with RR and the measurement of Ru mass in each cell by LA-ICP-MS offers higher precision compared to manually delimitation of the cell perimeter and eliminates the risk of biased information, which can be prone to inter–observer variability. The proposed procedure is fast and minimizes errors in cell area assignment when many cells are present in a slide. Additionally, it offers the possibility to carry out a faster data treatment approach if just relative volumes are compared, which can be advantageous for specific applications. However, it is important to highlight that assuring thickness gelatin homogeneity is critical to obtain accurate values with this methodology.

Furthermore, this approach allows for the acquisition of accurate information on the compositional distribution of a specific protein inside the cell, just by overlapping the Ru and Rh signals with the element of the corresponding protein label. This capability is particularly promising for ToF mass analyzers, making possible the simultaneous quantitative imaging of multiple proteins labelled with different elemental tags. Therefore, we believe that this work warrants further promising research for studies with other biomolecules or other cell cultures.

CRediT authorship contribution statement

Paula Menero-Valdés: Writing – original draft, Formal analysis, Data curation. **Lydia Álvarez:** Visualization, Resources. **Héctor González-Iglesias:** Visualization, Data curation. **Beatriz Fernández:** Writing – review & editing, Supervision, Funding acquisition, Conceptualization. **Rosario Pereiro:** Writing – review & editing, Supervision, Resources, Project administration, Funding acquisition.

Declaration of competing interest

The authors declare that they have no known competing financial interests or personal relationships that could have appeared to influence the work reported in this paper.

Data availability

Data will be made available on request.

Acknowledgements

This work was financially supported through project Ref. PID2022-137319OB-C21 (funded by MCIN/AEI/10.13039/501100011033/). P. Menero-Valdés acknowledges the FPU Grant with ref. FPU19/00556 (Ministry of Education, Spain). Authors would like to acknowledge María González-Fernández for conducting the initial optimization analyses using LA-ICP-MS as part of her undergraduate chemistry project. Additionally, we acknowledge the technical support offered by the Scientific and Technical Services (SCTs) at the University of Oviedo. L. Alvarez acknowledges the Fundación Rafael del Pino (http://www.frdelpino.es), through the "Cátedra Rafael del Pino".

Appendix A. Supplementary data

Supplementary data to this article can be found online at https://doi.org/10.1016/j.aca.2024.342906.

References

[1] J.L. Sterneckert, P. Reinhardt, H.R. Schöler, Investigating human disease using stem cell models, Nat. Rev. Gen. 15 (2014) 625–639, https://doi.org/10.1038/nrg3764.

[2] C. Davison, D. Beste, M. Bailey, M. Felipe-Sotelo, Expanding the boundaries of atomic spectroscopy at the single-cell level: critical review of SP-ICP-MS, LIBS and LA-ICP-MS advances for the elemental analysis of tissues and single cells, Anal. Bioanal. Chem. 415 (2023) 6931–6950, https://doi.org/10.1007/s00216-023-04721-8.

[3] H. Lu, H. Zhang, L. Li, Chemical tagging mass spectrometry: an approach for single-cell omics, Anal. Bioanal. Chem. 415 (2023) 6901–6913, https://doi.org/10.1007/s00216-023-04850-0.

[4] A. Lores-Padín, E. Mavrakis, B. Fernández, M. García, H. González-Iglesias, R. Pereiro, S.A. Pergantis, Gold nanoclusters as elemental label for the sequential quantification of apolipoprotein E and metallothionein 2A in individual human cells of the retinal pigment epithelium using single cell-ICP-MS, Anal. Chim. Acta 1203 (2022) 339701, https://doi.org/10.1016/j.aca.2022.339701.

[5] P. Menero-Valdés, A. Lores-Padín, B. Fernández, C.D. Quarles, M. García, H. González-Iglesias, R. Pereiro, Determination and localization of specific proteins in individual ARPE-19 cells by single cell and laser ablation ICP-MS using iridium nanoclusters as label, Talanta 253 (2023) 123974, https://doi.org/10.1016/j.talanta.2022.123974.

[6] M. Guo, A.F. Pegoraro, A. Mao, E.H. Zhou, P.R. Arany, Y. Hana, D.T. Burnette, M. H. Jensen, K.E. Kasza, J.R. Moore, F.C. Mackintosh, J.J. Fredberg, D.J. Mooney, J. Lippincott-Schwartz, D.A. Weitz, Cell volume change through water efflux impacts cell stiffness and stem cell fate, Proc. Natl. Acad. Sci. 41 (2017) E8618–E8627, https://doi.org/10.1073/pnas.1705179114.

[7] M.C. Lanz, E. Zatulovskiy, M.P. Swaffer, L. Zhang, I. Ilerten, S. Zhang, D. Shin-You, G. Marinov, P. McAlpine, J.E. Elias, J.M. Skotheim, Increasing cell size remodels the proteome and promotes senescence, Mol. Cel. 82 (2022) 3255–3269, https://doi.org/10.1016/j.molcel.2022.07.017.

[8] E. Zatulovskiy, M.C. Lanz, S. Zhang, F. McCarthy, J.E. Elias, J.M. Skotheim, Delineation of proteome changes driven by cell size and growth rate, Front. Cell Dev. Biol. 10 (2022) 980721, https://doi.org/10.3389/fcell.2022.980721.

[9] M. Resano, M. Aramendía, E. García-Ruiz, A. Bazo, E. Bolea-Fernández, F. Vanhaecke, Living in a transient world: ICP-MS reinvented via time-resolved analysis for monitoring single events, Chem. Sci. 13 (2022) 4436–4473, https://doi.org/10.1039/D1SC05452J.

[10] S. Theiner, K. Loehr, G. Koellensperger, L. Mueller, N. Jakubowski, Single-cell analysis by use of ICP-MS, J. Anal. At. Spectrom. 35 (2020) 1784–1813, https://doi.org/10.1039/D0JA00194E.

[11] A.B. Santos da Silva, M.A.Z. Arruda, Single-cell ICP-MS to address the role of trace elements at a cellular level, J. Trace Elem. Med. Biol. 75 (2023) 127086, https://doi.org/10.1016/j.jtemb.2022.127086.

[12] H. Lu, H. Zhang, L. Li, Chemical tagging mass spectrometry: an approach for single-cell omics, Anal. Bioanal. Chem. 415 (2023) 6901–6913, https://doi.org/10.1007/s00216-023-04850-0.

[13] W. Qin, H.J. Stärk, T. Reemtsma, Ruthenium red: a highly efficient and versatile cell staining agent for single-cell analysis using inductively coupled plasma time-of-flight mass spectrometry, Analyst 146 (2021) 6753–6759, https://doi.org/10.1039/D1AN01143J.

[14] M.A. Rapsomaniki, X.K. Lun, S. Woerner, M. Laumanns, B. Bodenmiller, M. Rodríguez-Martínez, CellCycleTRACER accounts for cell cycle and volume in mass cytometry data, Nat. Com 9 (2018) 632, https://doi.org/10.1038/s41467-018-03005-5.

[15] P. Menero-Valdés, M.I. Chronakis, B. Fernández, C.D. Quarles, H. González, B. Meermann, R. Pereiro, Single cell–ICP–ToF-MS for the multiplexed determination of proteins: evaluation of the cellular stress response, Anal. Chem. 95 (2023) 13322–13329, https://doi.org/10.1021/acs.analchem.3c02558.

[16] M. Cruz-Alonso, B. Fernandez, L. Álvarez, H. González-Iglesias, H. Traub, N. Jakubowski, R. Pereiro, Bioimaging of metallothioneins in ocular tissue sections by laser ablation-ICP-MS using bioconjugated gold nanoclusters as specific tags, Microchim. Acta 185 (2018) 64, https://doi.org/10.1007/s00604-017-2597-1.

[17] T. Van Helden, S. Braeuer, T. Van Acker, O. Leroux, D. Van Der Straeten, F. Vanhaecke, High-speed mapping of Hg and Se in biological tissue via laser ablation-inductively coupled plasma-mass spectrometry, J. Anal. At. Spectrom. 37 (2022) 1455–1461, https://doi.org/10.1039/D2JA00131D.

[18] P.A. Doble, R. Gonzalez de Vega, D.P. Bishop, D.J. Hare, D. Clases, Laser ablation–inductively coupled plasma–mass spectrometry imaging in biology, Chem. Rev. 121 (2021) 11769–11822, https://doi.org/10.1021/acs.chemrev.0c01219.

[19] R. Delfino, M. Biasotto, R. Candido, M. Altissimo, M. Stebel, M. Salomè, J.T. van Elteren, K.V. Mikuš, C. Zennaro, M. Šala, R. Addobbati, G. Tromba, L. Pascolo, Gadolinium tissue deposition in the periodontal ligament of mice with reduced renal function exposed to Gd-based contrast agents, Toxicol. Lett. 301 (2019) 157–167, https://doi.org/10.1016/j.toxlet.2018.11.014.

[20] T. Van Acker, T. Buckle, S.J.M. Van Malderen, D.M. van Willigen, V. van Unen, F. W.B. van Leeuwen, F. Vanhaecke, High-resolution imaging and single-cell analysis via laser ablation-inductively coupled plasma-mass spectrometry for the determination of membranous receptor expression levels in breast cancer cell lines using receptor-specific hybrid tracers, Anal. Chim. Acta 1074 (2019) 43–53, https://doi.org/10.1016/j.aca.2019.04.064.

[21] A. Lores-Padín, P. Menero-Valdés, B. Fernández, R. Pereiro, Nanoparticles as labels of specific-recognition reactions for the determination of biomolecules by

inductively coupled plasma-mass spectrometry, Anal. Chim. Acta 1128 (2020) 251–268.
[22] C. Davison, D. Beste, M. Bailey, M. Felipe-Sotelo, Expanding the boundaries of atomic spectroscopy at the single-cell level: critical review of SP-ICP-MS, LIBS and LA-ICP-MS advances for the elemental analysis of tissues and single cells, Anal. Bioanal. Chem. 415 (2023) 6931–6950, https://doi.org/10.1007/s00216-023-04721-8.
[23] K. Mervic, M. Šala, S. Theiner, Calibration approaches in laser ablation inductively coupled plasma mass, Trends Anal. Chem. 172 (2024) 117574, https://doi.org/10.1016/j.trac.2024.117574.
[24] S.J.M. Van Malderen, E. Vergucht, M. De Rijcke, C. Janssen, L. Vincze, F. Vanhaecke, Quantitative determination and Subcellular imaging of Cu in single cells via laser ablation-ICP-mass spectrometry using high-density Microarray gelatin standards, Anal. Chem. 88 (11) (2016) 5583–5587, https://doi.org/10.1021/acs.analchem.6b00334.
[25] L. Mueller, A.J. Herrmann, S. Techritz, U. Panne, N. Jakubowski, Quantitative characterization of single cells by use of immunocytochemistry combined with multiplex LA-ICP-MS, Anal. Bioanal. Chem. 409 (2017) 3667–3676, https://doi.org/10.1007/s00216-017-0310-1.
[26] K. Löhr, H. Traub, A.J. Wanka, U. Panne, N. Jakubowski, Quantification of metals in single cells by LA-ICP-MS: comparison of single spot analysis and imaging, J. Anal. At. Spectrom 33 (2018) 1579–1587, https://doi.org/10.1039/C8JA00191J.
[27] K. Löhr, O. Borovinskaya, G. Tourniaire, U. Panne, N. Jakubowski, Arraying of single cells for quantitative high Throughput laser ablation ICP-TOF-MS, Anal. Chem. 91 (18) (2019) 11520–11528, https://doi.org/10.1021/acs.analchem.9b00198.
[28] A. Lores-Padin, B. Fernández, M. García, H. González-Iglesias, R. Pereiro, Real matrix-matched standards for quantitative bioimaging of cytosolic proteins in individual cells using metal nanoclusters as immunoprobes-label: a case study using laser ablation ICP-MS detection, Anal. Chim. Acta 1221 (2022) 340128, https://doi.org/10.1016/j.aca.2022.340128.
[29] L. Zheng, L. Feng, J. Shi, H. Chen, B. Wang, M. Wang, H. Wang, W. Feng, Single-cell isotope dilution analysis with LA–ICP–MS: a new approach for quantification of nanoparticles in single cells, Anal. Chem. 92 (21) (2020) 14339–14345, https://doi.org/10.1021/acs.analchem.0c01775.
[30] W. Luo, F. Dong, M. Wang, T. Li, Y. Wang, W. Dai, J. Zhang, C. Jiao, Z. Song, J. Shen, Y. Ma, Y. Ding, F. Yang, Z. Zhang, X. He, Particulate standard establishment for absolute quantification of nanoparticles by LA-ICP-MS, Anal. Chem. 95 (2023) 6391–6398, https://doi.org/10.1021/acs.analchem.3c00028.
[31] S.J.M. Van Malderen, T. Van Acker, B. Laforce, M. De Bruyne, R. De Rycke, T. Asaoka, L. Vincze, F. Vanhaecke, Three-dimensional reconstruction of the distribution of elemental tags in single cells using laser ablation ICP-mass spectrometry via registration approaches, Anal. Bioanal. Chem. 411 (2019) 4849–4859, https://doi.org/10.1007/s00216-019-01677-6.
[32] K. Dunn, A. Aotaki-Keen, F. Putkey, L. Hjelmeland, ARPE-19, a human retinal pigment epithelial cell line with differentiated properties, Exp. Eye Res. 62 (1996) 155–170, https://doi.org/10.1006/exer.1996.0020.
[33] H.S. Alsaif, A.O. Khan, N. Patel, H. Alkuraya, M. Hashem, F. Abdulwahab, N. Ibrahim, M.A. Aldahmesh, F.S. Alkuraya, Congenital glaucoma and CYP1B1: an old story revisited, Hum. Genet. 138 (2019) 8–9, https://doi.org/10.1007/s00439-018-1878-z.
[34] Y. Tang, E.A. Scheef, S. Wang, C.M. Sorenson, C.B. Marcus, C.R. Jefcoate, N. Sheibani, CYP1B1 expression promotes the proangiogenic phenotype of endothelium through decreased intracellular oxidative stress and thrombospondin-2 expression, Blood 113 (2009) 744–754, https://doi.org/10.1182/blood-2008-03-145219.
[35] Y.S. Song, A.J. Annalora, C.B. Marcus, C.R. Jefcoate, C.M. Sorenson, N. Sheibani, Cytochrome P450 1B1: a key Regulator of ocular iron homeostasis and oxidative stress, Cells 11 (2022) 2930, https://doi.org/10.3390/cells11192930.
[36] M. Cruz-Alonso, B. Fernández, M. García, H. González-Iglesias, R. Pereiro, Quantitative imaging of specific proteins in the human retina by laser ablation ICPMS using bioconjugated metal nanoclusters as labels, Anal. Chem. 90 (2018) 12145–12151. https://pubs.acs.org/doi/10.1021/acs.analchem.8b03124.
[37] S. Dahan, J.P. Ahluwalia, L. Wong, B.I. Posner, J.J. Bergeron, Concentration of intracellular hepatic apolipoprotein E in Golgi apparatus saccular distensions and endosomes, J. Cell Biol. 127 (1994) 1859–1869, https://doi.org/10.1083/jcb.127.6.1859.
[38] R. Dierichs, Ruthenium red as a stain for electron microscopy. Some new aspects of its application and mode of action, Histochemistry 64 (1979) 171–187, https://doi.org/10.1007/BF00490097.
[39] L.N. Waller, N. Fox, K.F. Fox, A. Fox, R.L. Price, Ruthenium red staining for ultrastructural visualization of a glycoprotein layer surrounding the spore of Bacillus anthracis and Bacillus subtilis, J. Microbiol. Methods 58 (2004) 23–30, https://doi.org/10.1016/j.mimet.2004.02.012.
[40] A.L. Kiss, E. Botos, Endocytosis via caveolae: alternative pathway with distinct cellular compartments to avoid lysosomal degradation? J. Cell Mol. Med. 13 (2009) 1228–1237, https://doi.org/10.1111/j.1582-4934.2009.00754.x.